PROCEEDINGS OF SCIENCE

Probability distributions for UHECR propagation

Leonel Morejon[a,*]

[a] *Bergische Universität Wuppertal,*
Gaußstraße 20, 42103 Wuppertal, Germany

E-mail: leonel.morejon@uni-wuppertal.de

Results from the Pierre Auger Observatory indicate that nuclei make a sizeable part of the observed flux of ultra-high energy cosmic rays (UHECRs). The theoretical study of both in-source and extra-galactic propagation requires detailed understanding of nuclear interactions with the surrounding photon fields (*i.e.* CMB, EBL, accretion disk thermal emission, non-thermal emissions) and in particular the resulting nuclear cascades which describe the escaping composition and its evolution over propagation. This contribution presents a novel treatment of UHECR nuclear cascades as a Continuous Time Markov Chain showing that this process underlies the stochastic photonuclear interactions experienced by UHECRs both within sources and during extra-galactic propagation. As result, expressions for probability distributions are obtained which have closed form and are more efficient to compute than other methods presently employed such as Monte-Carlo or numerical integration of systems of differential equations. Furthermore, this approach allows more nuance in describing compositions without the need of ad-hoc restrictions (such as limiting the number of species by decay lifetime or restricting products to most frequent secondaries) expanding the number of nuclear species that can be included with low cost in computation time. Using this method, the propagation horizon related to photointeractions is defined precisely and can be quantified to any desired level of confidence using the obtained probability density functions for complete disintegration. The in-source survival fraction is computed in an example of UHECR source previously studied, and the application of this approach for extra-galactic propagation is also discussed.

38th International Cosmic Ray Conference (ICRC2023)
26 July - 3 August, 2023
Nagoya, Japan

*Speaker

PoS(ICRC2023)284

Contents

1. Introduction

The origin of UHECRs and the connections to other messengers are intricately linked to their interactions within the sources and through the propagations over intergalactic distances. The increasingly compelling evidence of a heavier composition in UHECRs increases the complexity because, besides protons, a large number of nuclear species is needed to characterize the UHECR composition, although in the present only long-lived nuclei up to iron are considered. To address this issue, different numerical codes (*e.g.* [1–4]) have been suited with the necessary interaction types (electron pair production[5] photodisintegration [1], photopion [6]) that account for the conversions between nuclear species and continuous energy losses (CEL). The stochastic nature of some of these interactions and its non-negligible effect on the results has been recognized and studied via Monte Carlo simulations [1–3]. However, other approaches assuming continuous approximation for these stochastic processes have been employed in analogy to CEL [4, 7–9] and achieved reasonable agreement with the average values of the quantities of interest. These codes have been successfully employed to compute the observed composition based on assumptions about the sources, hence providing limits for the parameters related to the source evolution and spectral index under reasonable assumptions. Nevertheless, the detailed understanding of the cascades has been limited because of their complexity, and the large number of parameters employed in their description: for example no closed form of the distance distributions has been presented although they have been computed using Monte Carlo simulations (*e.g.* [10]) and with analytical expressions derived under the assumption of some continuous approximation of the stochastic interactions (*e.g.* [7, 9]). This paper presents a novel approach to describe the nuclear cascades which implicitly accounts for its stochastic nature and applies to both UHECR sources and extra-galactic propagation. Some of its advantages include its comprehensibility and the ease of implementation and computation. Furthermore, it provides the possibility of studying the statistical fluctuations inherent to the cascades. The probability distributions of the UHECR composition evolution are obtained as closed form expressions and examples of these distributions are presented for in-source and for extra-galactic propagation. The in-source survival fraction is computed employing a previously studied UHECR source scenario. The extra-galactic propagation employing this approach is discussed establishing limiting cases on account of the relative importance of CEL.

2. Formulation of nuclear cascades as a Markov process

The transformations between UHECRs of different nuclear species are governed by interaction rates (number of interaction per unit length) [11]

$$\lambda(\gamma, z) = \frac{1}{2\gamma^2}\int_0^\infty \frac{n(\epsilon, z)}{\epsilon^2} d\epsilon \int_0^{2\epsilon\gamma} \varepsilon\sigma(\varepsilon) d\varepsilon \tag{1}$$

where $\varepsilon = \gamma\epsilon(1 - \cos\theta)$ is the photon energy boosted to the nucleus reference frame, and σ represents the cross section for interaction of interest: for photodisintegration interactions σ includes the Giant Dipole Resonance [12] and the quasi-deuteron [13] modes of interaction; for photomeson interactions σ is predominantly the photopion production cross section [6].

Both photodisintegration and photomeson interactions lead to the breakup of the initial nucleus into species of lower mass, all preserving the initial Lorentz boost except the secondaries of lower masses (pions and resulting neutrinos and photons) whose energy distribution is broader. These interactions are stochastic not only on the position/time of occurrence, but also on the number and species of the secondaries produced in each event. However, the probabilities of production are governed by the interaction rates and are constant[1] as the cascade develops, making this is a stochastic Markov process and the cascade a Continuous Time Markov Chain[14]. The probability distribution of the distance until absorption L (*i.e.* reaching a set state, or nuclear species in this case) has been derived and is in this case [14]

$$f(L) = \boldsymbol{\alpha_0} \exp(\boldsymbol{\Lambda} L)\, \boldsymbol{\Lambda e} \tag{2}$$

where $\boldsymbol{\Lambda} = \boldsymbol{\Lambda}(\gamma)$ is a matrix formed by all the interaction rates of all species ($\{S_k\}, k = 1..N$)

$$\boldsymbol{\Lambda}(\gamma) = \begin{pmatrix} -\lambda^{\rm tot}_{S_1} & \lambda_{S_1\to S_2} & \lambda_{S_1\to S_3} & \lambda_{S_1\to S_4} & \lambda_{S_1\to S_5} & \dots & \lambda_{S_1\to S_N} \\ 0 & -\lambda^{\rm tot}_{S_2} & \lambda_{S_2\to S_2} & \lambda_{S_2\to S_3} & \lambda_{S_2\to S_4} & \dots & \lambda_{S_2\to S_N} \\ 0 & 0 & -\lambda^{\rm tot}_{S_3} & \lambda_{S_3\to S_3} & \lambda_{S_3\to S_3} & \dots & \lambda_{S_3\to S_N} \\ \dots & \dots & \dots & \dots & \dots & \dots & \dots \\ 0 & 0 & 0 & 0 & 0 & \dots & -\lambda^{\rm tot}_{S_N} \end{pmatrix} \tag{3}$$

included in the cascade and $\boldsymbol{\alpha}$ is a vector whose elements are the starting fractions of each of the N species. The rates $\lambda_{S_i\to S_j}$ are obtained using Eq. 1 with the corresponding cross section where the interacting species S_i produces S_j, and $\lambda^{\rm tot}_{S_i} = \sum_{j=i+1}^{N} \lambda_{S_i\to S_j}$. Note that $\boldsymbol{\Lambda}$ is upper triangular when the nuclear species are arranged in monotonically decreasing order of the mass ($A_m \geq A_n$ as long as $m < n$). Finally, employing Kolmogorov's differential equations [14] the evolution of the probability vector describing the fractions of each species can be written

$$\boldsymbol{\alpha}(L) = \boldsymbol{\alpha_0} \exp(\boldsymbol{\Lambda} L)\ . \tag{4}$$

3. Source propagation

The cascade of nuclei inside sources has been studied with diffusion equations analogous to the extragalactic propagation case [15–17] as interactions with photons are expected to be dominant.

[1] Interaction rates depend on the redshift only for propagations over sufficiently large distances, however in this case a small modification yields an analogous form of Eq. 2 (see Section 4).

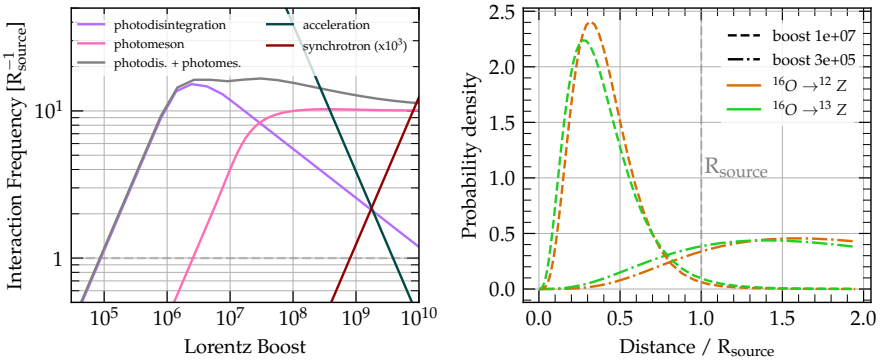

Figure 1: Example of nuclear disintegration in a source scenario (see text). The interaction rates of the injected oxygen (left) and the probability distributions over distance for some secondary nuclei at two different boosts as indicated (right).

However, the photon densities in such scenarios are better modelled with a broken power law [17, 18]. Figure 1 (left) shows the interaction rates for the injected species (oxygen) in a Tidal Disruption Event source type modelled as in Refs. [6, 18] where the photodisintegration and photomeson interactions are clearly dominant over all boosts compared to CEL (synchrotron losses in this case). The acceleration rate is also shown to remark the maximal boost of escaping nuclei as the point where the acceleration rate is matched by all the losses ($\gamma_{\rm max} \approx 3 \cdot 10^8$).

The probability distributions for the loss of three (green lines) and for the loss of four nucleons (orange lines) by the injected nucleus oxygen according to Eq. 2 are shown in Figure 1 (right). The distributions are shown for two values of the Lorentz boost for comparison. At $\gamma = 3 \cdot 10^5$ the injected nuclei would interact in average about three times before escaping the source, although half of the rate leads to a one-neutron loss and the other half to one-proton loss. The resulting species from each subsequent interaction have in general different interaction rates but typically smaller than the more massive injected species. The distributions for the loss of three and four nucleons both peak at distances larger than the source radius which illustrates their broadness. However, the external portion should be truncated since nuclei are assumed to escape beyond a distance equal to the radius. Integrating the distributions up to the this limit yields the probabilities that a certain loss of mass has occurred before the escape: 16.4 % for three nucleons less and 11.5 % for four nucleons less. These results reflect the natural expectation that the loss of four nucleons is less likely since in average it is conditioned by the loss of three nucleons. It should be noted that these probabilities only reflect the likelihood of mass loss before versus after crossing the radius (if the target photons are the same), they do not reflect probabilities related to the composition distribution, which may be computed with Eq. 4

On the other hand, for $\gamma = 1 \cdot 10^7$ the interaction frequency is about five times larger than at $\gamma = 3 \cdot 10^5$ hence leading to a considerable suppression: the probability of three-nucleon before escape is 98.2 % whereas the probability of four-nucleon loss before escape is 99.1 %! This apparently contradictory result is a consequence of the difference in the tails of these curves: while the four-nucleon loss curve peaks at a larger distance (as expected given the average conditional loss of three nucleons) its tail decreases faster. The tail of the curve is strongly influenced by the interaction rates of the ending species, and in this case the mean rate for species with $A = 12$ is

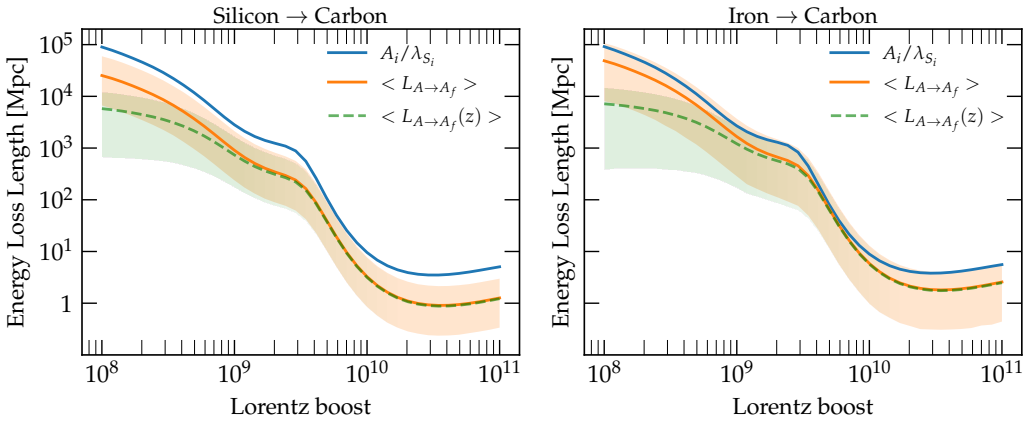

Figure 2: Characteristic propagation distances compared with the energy loss lengths as a function of Lorentz boost for two different starting nuclear species (see the text for details).

$11.38\, R^{-1}_{\rm source}$, larger than the mean rate for species with $A = 13$ is $10.43\, R^{-1}_{\rm source}$ therefore in a sense $A = 12$ have in average a shorter reach compared to $A = 13$ species.

4. Extragalactic propagation

4.1 Propagation horizons

In the case of extragalactic propagation the interaction rates are also dependent on redshift due to the corresponding dependence of the target photon fields, and thus the interaction matrix can't be considered invariable over the propagation path. This means that the process no longer respects the Markov property but depends on the whole preceding path. However, this is a special case where the Markov property can be recovered[19] because the rates scale as $\lambda(\gamma, z) = (1+z)^3\lambda((1+z)\gamma, z = 0)$ [20] so the interaction matrix can be written $\mathbf{\Lambda} \approx (1+z)^3\mathbf{\Lambda}(\gamma)$ to a first approximation and the obtained distribution resembles the expression in Eq. 2 [19]

$$f(L) = (1+z(L))^3\boldsymbol{\alpha_0}\exp\left(\mathbf{\Lambda}\int_0^L (1+z(s))^3 ds\right)\mathbf{\Lambda e} \tag{5}$$

Figure 2 shows the means (lines) and the 50 % confidence bands (shaded areas) of the distance distributions for cascades silicon-to-carbon (left) and iron-to-carbon (right) computed using Equation 2 (orange) and Equation 5 (green). The distributions are indistinguishable when the distances are small ($L \lesssim 100$ Mpc) reflecting that the expressions are identical for $z \approx 0$, whereas they diverge more as the propagation distance corresponds to larger redshitfs. For comparison, the blue line shows the energy loss length $\mathcal{D}_i = \left(\frac{1}{E_i}\frac{dE_i}{dL}\right)^{-1} = \left(\frac{1}{A_i}\frac{dA_i}{dL}\right)^{-1} = \left(\frac{1}{A_i}\sum_j (A_i - A_j)\lambda_{S_i\to S_j}\right)^{-1}$ [1, 11] which is commonly employed to estimate the typical propagation distance of UHECRs (it reduces to $\mathcal{D}_i \approx \frac{A_i}{\lambda_{S_i}}$ when one nucleon emission is the dominant loss). Overall $\mathcal{D}_i$ is larger than the means from the distributions in Eqs. 2- 5 and thus overestimates the characteristic propagation distance, especially if we note that the loss of $(A_i - 12)$ nucleons requires a total distance $\frac{(A_i-12)}{\tilde{n}_i}\mathcal{D}_i$ where $\tilde{n}_i$ is the average number of nucleons lost per energy loss length $\tilde{n}_i = \sum_j (A_i - A_j)\frac{\lambda_{S_i\to S_j}}{\lambda_{S_i}}$. Therefore,

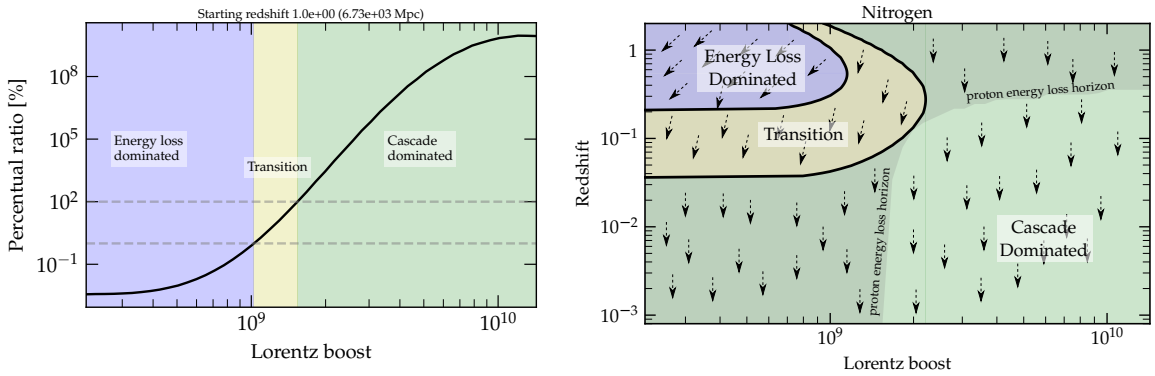

Figure 3: The description of the propagation can be divided in three portions according to the dominant process (see the text for details).

$\mathcal{D}_i$ is not as good estimate of the characteristic propagation distances as the mean of the distributions presented here.

4.2 Continuous Energy Losses and propagation regimes

Another aspect of extra-galactic propagation is the effect of CEL which produce boost changes as nuclei propagate and thus the Markov property of the cascade process does not hold, however it is useful to determine the conditions in which the effect of the CEL can be neglected.

The Taylor expansion of the rates to the first order approximation around set values $\gamma = \gamma_0$, $z = z_0$ is

$$\lambda(\gamma, z) \approx \lambda(\gamma_0, z_0) + \left.\frac{\partial\lambda}{\partial\gamma}\right|_{\gamma_0,\, z_0} (\gamma - \gamma_0) + \left.\frac{\partial\lambda}{\partial z}\right|_{\gamma_0,\, z_0} (z - z_0) = \lambda(\gamma_0, z_0) + \left(\frac{\partial\lambda}{\partial\gamma}\frac{\partial\gamma}{\partial z} + \frac{\partial\lambda}{\partial z}\right)(z - z_0) \tag{6}$$

where $(\gamma - \gamma_0) = \frac{\partial\lambda}{\partial z}(z - z_0)$ was used and $\lambda(\gamma_0, z_0)$, $\frac{\partial\lambda}{\partial\gamma}$ and $\frac{\partial\lambda}{\partial z}$ can be obtained from Eq. 1, and $\frac{\partial\gamma}{\partial z}$ has the form [7]

$$\frac{d\gamma}{dz} = \frac{\gamma}{1+z}\left(1 + \frac{\beta_{\text{pair}}}{H(z)}\right). \tag{7}$$

From Eq.6 is clear that the fraction $\eta = \lambda(\gamma_0, z_0)/\left(\frac{\partial\lambda}{\partial\gamma}\frac{\partial\gamma}{\partial z} + \frac{\partial\lambda}{\partial z}\right)/(z - z_0)$ determines the dominant term and can help determine a validity region given a choice of threshold value and a fixed step in redshift. When $\eta >> 1$ the main term is $\lambda(\gamma_0, z_0)$ and the effect of CEL can be neglected, thus this determines the *Cascade Dominated* regime where the distributions Eq. 2 and Eq. 5 apply. For $\eta << 1$ the effect of CEL is prevalent and $\lambda(\gamma_0, z_0)$ is subdominant, thus this determines the *Energy Loss Dominated* regime where the cascade cannot occur because the energy losses produce a decrease in boost at a larger rate and at lower values of the boost $\lambda(\gamma, z)$ is increasingly lower. An intermediate *Transition* regime can be defined delimited by $1/\xi \leq \eta \leq \xi$ where a suitable threshold ξ specifies the desired precision. Figure 3 (left) illustrates these regimes as delimited by the values of η for $z = 1$: *Energy Loss Dominated* regime in blue, *Cascade Dominated* regime in green and the *Transition* regime in yellow. Computing these boundaries for a range of redshifts a γ - z phase space is obtained as represented in Figure 3 (right) where arrows illustrate the approximate paths followed at different points. We can think of the propagation in simplified form depending on where

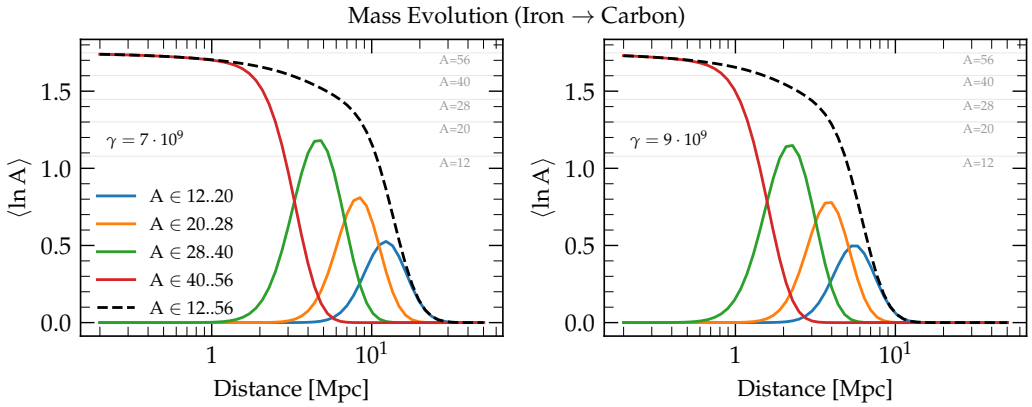

Figure 4: Example of extragalactic propagation of iron after escaping the source. The inclusive distributions of $\langle \ln A \rangle$ for different mass groups are shown for two different boost values as indicated.

the values (γ, z) of the starting cosmic ray fall in this phase space: a cosmic ray starting in the cascade dominated region will completely cascade without a change of boost (downwards vertical pathway) whereas starting in the energy loss region leads to paths running down and left while the initial species does not change but it suffers energy losses during propagation. In the transition zone, however, both the cascading and energy losses occur concurrently and different results may be expected depending on the evolution of η. The detailed analysis of the transition zone is left for future works but it should be noted that its description is possible employing the formalism for Inhomogeneous Continuous Time Markov Chains[21]. In any case, it is clear from Figure 3 (right) that the *Transition* regime is a limited portion of the propagation path even with considerable values of ξ, and if the path crosses to the *Cascade Dominated* regime the boost freezes and the cascades proceeds at the corresponding rates. Additionally, Figure 3 (right) delimits the phase space with a darkened region to illustrate the limits for proton propagation indicating that protons starting in this region of the phase space will lose enough energy to fall outside of the range of UHECRs before reaching the Earth. This proton energy loss horizon also limits the secondaries from nitrogen that can reach Earth, since for nitrogen nuclei starting in this region only secondaries heavier than protons will make it and if it cascades completely within this region then non of the secondaries reach the Earth as UHECRs.

Figure 4 shows an example of propagation of UHECRs as a function of the distance from the source assuming $z_0 \approx 0$, hence in the *Cascade Dominated* regime and following Eq. 2. The different curves represent the evolution of mean $\langle \ln A \rangle$ of different mass groups as a function of distance with each panel showing one of two different values of Lorentz boost as indicated. The injected species is iron and the "absorbing" species is carbon and the interaction rates employed have been taken from the tabulated values of interaction rates employed by CRPropa which include 184 nuclei and both photodisintegration and photomeson interactions[20]. The distributions at different boosts are remarkably similar, mostly differing on the distance range over which the cascade develops. This may be explained by a smooth change of the interaction matrix with the boost $\mathbf{\Lambda}(\gamma = 7 \cdot 10^9) \propto \mathbf{\Lambda}(\gamma = 9 \cdot 10^9)$ and could be the reason for the so called *Disciplined Disintegration* described in [22].

Acknowledgements

This work has received funding via the grant MultI-messenger probe of Cosmic Ray Origins (MICRO) from the DFG through project number 445990517.

References

[1] J.L. Puget, F.W. Stecker and J.H. Bredekamp, *Photonuclear interactions of ultrahigh energy cosmic rays and their astrophysical consequences*, *The Astrophysical Journal* **205** (1976) 638.
[2] E. Armengaud, G. Sigl, T. Beau and F. Miniati, *Crpropa: A numerical tool for the propagation of uhe cosmic rays, -rays and neutrinos*, *Astroparticle Physics* **28** (2007) 463.
[3] R. Aloisio, D. Boncioli, A. Grillo, S. Petrera and F. Salamida, *Simprop: a simulation code for ultra high energy cosmic ray propagation*, *Journal of Cosmology and Astroparticle Physics* **2012** (2012) 007.
[4] J. Heinze, A. Fedynitch, D. Boncioli and W. Winter, *A new view on auger data and cosmogenic neutrinos in light of different nuclear disintegration and air-shower models*, *The Astrophysical Journal* **873** (2019) 88.
[5] G.R. Blumenthal, *Energy loss of high-energy cosmic rays in pair-producing collisions with ambient photons*, *Physical Review D* **1** (1970) 1596.
[6] L. Morejon, A. Fedynitch, D. Boncioli, D. Biehl and W. Winter, *Improved photomeson model for interactions of cosmic ray nuclei*, *Journal of Cosmology and Astroparticle Physics* **2019** (2019) 007.
[7] R. Aloisio, V. Berezinsky and S. Grigorieva, *Analytic calculations of the spectra of ultra-high energy cosmic ray nuclei. i. the case of cmb radiation*, *Astroparticle Physics* **41** (2013) 73.
[8] O.E. Kalashev and E. Kido, *Simulations of ultra-high-energy cosmic rays propagation*, *Journal of Experimental and Theoretical Physics* **120** (2015) 790.
[9] D. Hooper, S. Sarkar and A.M. Taylor, *Intergalactic propagation of ultrahigh energy cosmic ray nuclei: An analytic approach*, *Physical Review D* **77** (2008) 103007.
[10] G. Bertone, C. Isola, M. Lemoine and G. Sigl, *Ultrahigh energy heavy nuclei propagation in extragalactic magnetic fields*, *Physical Review D* **66** (2002) 103003.
[11] F.W. Stecker and M.H. Salamon, *Photodisintegration of ultra–high-energy cosmic rays: A new determination*, *The Astrophysical Journal* **512** (1999) 521.
[12] V. Plujko, O. Gorbachenko, R. Capote and P. Dimitriou, *Giant dipole resonance parameters of ground-state photoabsorption: Experimental values with uncertainties*, *Atomic Data and Nuclear Data Tables* **123-124** (2018) 1.
[13] J.S. Levinger, *The high energy nuclear photoeffect*, *Physical Review* **84** (1951) 43.
[14] M. Bladt and B.F. Nielsen, *Matrix-Exponential Distributions in Applied Probability*, vol. 81, Springer US (2017), 10.1007/978-1-4939-7049-0.
[15] D. Boncioli, A. Fedynitch and W. Winter, *Nuclear physics meets the sources of the ultra-high energy cosmic rays*, *Scientific Reports* **7** (2017) 4882.
[16] X. Rodrigues, A. Fedynitch, S. Gao, D. Boncioli and W. Winter, *Neutrinos and ultra-high-energy cosmic-ray nuclei from blazars*, *The Astrophysical Journal* **854** (2018) 54.
[17] D. Biehl, D. Boncioli, A. Fedynitch and W. Winter, *Cosmic ray and neutrino emission from gamma-ray bursts with a nuclear cascade*, *Astronomy Astrophysics* **611** (2018) A101.
[18] D. Biehl, D. Boncioli, C. Lunardini and W. Winter, *Tidally disrupted stars as a possible origin of both cosmic rays and neutrinos at the highest energies*, *Scientific Reports* **8** (2018) 10828.
[19] H. Albrecher and M. Bladt, *Inhomogeneous phase-type distributions and heavy tails*, *Journal of Applied Probability* **56** (2019) 1044.
[20] R.A. Batista, A. Dundovic, M. Erdmann, K.-H. Kampert, D. Kuempel, G. Müller et al., *Crpropa 3—a public astrophysical simulation framework for propagating extraterrestrial ultra-high energy particles*, *Journal of Cosmology and Astroparticle Physics* **2016** (2016) 038.
[21] M. Arns, P. Buchholz and A. Panchenko, *On the numerical analysis of inhomogeneous continuous-time markov chains*, *INFORMS Journal on Computing* **22** (2010) 416.
[22] L. Morejon, *New Interaction Models of Ultra-high-energy Cosmic Rays from a Nuclear Physics Approach*, Ph.D. thesis, Humboldt-Universität zu Berlin, 2020. DOI.